Unimpaired phase-sensitive amplification by vector four-wave mixing near the zero-dispersion frequency

C. J. McKinstrie,[1] S. Radic,[2] M. G. Raymer[3] and L. Schenato[4]

[1]*Bell Laboratories, Lucent Technologies, Holmdel, New Jersey 07733*
[2]*Department of Electrical and Computer Engineering, University of California at San Diego, La Jolla, California 92093*
[3]*Oregon Center for Optics and Department of Physics, University of Oregon, Eugene, Oregon 97403*
[4]*Department of Information Engineering, University of Padua, 35131 Padua, Italy*
mckinstrie@lucent.com

Abstract: Phase-sensitive amplification (PSA), which is produced by degenerate four-wave mixing (FWM) in a randomly-birefringent fiber, has the potential to improve the performance of optical communication systems. Scalar FWM, which is driven by parallel pumps, is impaired by the generation of pump–pump and pump–signal harmonics, which limit the level, and modify the phase sensitivity, of the signal gain. In contrast, vector FWM, which is driven by perpendicular pumps, is not impaired by the generation of harmonics. Vector FWM produces PSA with the classical properties of a one-mode squeezing transformation.

OCIS codes: (060.2320) fiber optics amplifiers and oscillators; (060.4370) nonlinear optics, fibers; (190.4380) nonlinear optics, four-wave mixing.

References and links

1. R. Loudon, "Theory of noise accumulation in linear optical-amplifier chains," IEEE J. Quantum Electron. **21**, 766–773 (1985).
2. Y. Mu and C. M. Savage, "Parametric amplifiers in phase-noise-limited optical communications," J. Opt. Soc. Am. B **9**, 65–70 (1992).
3. H. P. Yuen, "Reduction of quantum fluctuation and suppression of the Gordon–Haus effect with phase-sensitive linear amplifiers," Opt. Lett. **17**, 73–75 (1992).
4. R. D. Li, P. Kumar, W. L. Kath and J. N. Kutz, "Combating dispersion with parametric amplifiers," IEEE Photon. Technol. Lett. **5**, 669–672 (1993).
5. C. J. McKinstrie and S. Radic, "Phase-sensitive amplification in a fiber," Opt. Express **12**, 4973–4979 (2004).
6. C. J. McKinstrie, M. Yu, M. G. Raymer and S. Radic, "Quantum noise properties of parametric processes," Opt. Express **13**, 4986–5012 (2005).
7. C. J. McKinstrie, M. G. Raymer, S. Radic and M. V. Vasilyev, "Quantum mechanics of phase-sensitive amplification in a fiber," Opt. Commun. **257**, 146–163 (2006).
8. R. Loudon, *The Quantum Theory of Light, 3rd Edition* (Oxford University Press, 2000).
9. C. J. McKinstrie and M. G. Raymer, "Four-wave-mixing cascades near the zero-dispersion frequency," Opt. Express **14**, 9600–9610 (2006).
10. J. Fan and A. Migdall, "Phase-sensitive four-wave mixing and Raman suppression in a microstructure fiber with dual laser pumps," Opt. Lett. **31**, 2771–2773 (2006).
11. H. Kogelnik, R. M. Jopson and L. E. Nelson, "Polarization-mode dispersion," in *Optical Fiber Telecommunications IVB*, edited by I. P. Kaminow and T. Li (Academic, San Diego, 2002), pp. 725–861.
12. I. S. Gradsteyn and I. M. Ryzhik, *Tables of Integrals, Series and Products* (Academic Press, 1994), pp. 987–994.
13. K. Inoue, "Polarization effect on four-wave mixing efficiency in a single-mode fiber," IEEE J. Quantum Electron. **28**, 883–894 (1992).

#78120 - $15.00 USD Received 14 December 2006; revised 15 February 2007; accepted 15 February 2007

14. C. J. McKinstrie, H. Kogelnik, R. M. Jopson, S. Radic and A. V. Kanaev, "Four-wave mixing in fibers with random birefringence," Opt. Express **12**, 2033–2055 (2004).

1. Introduction

Long-haul communication systems require optical amplifiers to compensate for fiber loss. Current systems use erbium-doped or Raman fiber amplifiers. These amplifiers are examples of phase-insensitive amplifiers (PIAs), which produce signal gain that is independent of the signal phase. In principle, phase-sensitive amplifiers (PSAs) could also be used. The potential advantages of PSAs include, but are not limited to, noise reduction [1], the reduction of noise- and collision-induced phase [2] and frequency [3] fluctuations, and dispersion compensation [4].

Previous papers [5, 6, 7] showed that degenerate four-wave mixing (FWM) in a randomly-birefringent fiber (RBF) produces phase-sensitive amplification (PSA), provided that the signal frequency (ω_0) is the average of the pump frequencies (ω_{-1} and ω_1). Degenerate scalar and vector FWM are illustrated in Figs. 1(*a*) and 1(*b*), respectively. In the former process (inverse

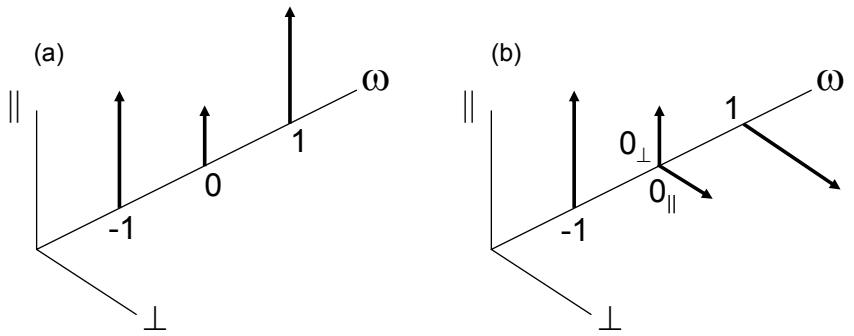

Fig. 1. Polarization diagrams for degenerate scalar FWM (left) and degenerate vector FWM (right).

modulation interaction) $\gamma_{-1}+\gamma_1 \rightarrow 2\gamma_0$, where γ_j represents a photon with frequency ω_j. In the latter process (degenerate phase conjugation) $\gamma_{-1}+\gamma_1 \rightarrow \gamma_{\|}+\gamma_{\perp}$, where the subscript 0 was omitted for simplicity.

If one assumes that each interaction involves only the aforementioned pumps and signal, then each interaction produces PSA with the classical properties of a one-mode squeezing transformation [8]. FWM processes are driven by pump- and signal-induced nonlinearities and limited by dispersion-induced wavenumber shifts. If the pump frequencies differ significantly, strong dispersion prevents other (secondary) FWM processes from occurring and the preceding assumption is valid. However, it is difficult to phase lock pumps with dissimilar frequencies, which are usually produced by two separate lasers. In contrast, it is easy to phase lock pumps with similar frequencies, which can be produced by one laser and a phase modulator. However, if the pump frequencies are similar, dispersion is too weak to counter nonlinearity and secondary FWM processes occur.

A previous paper on scalar FWM [9] showed that, if the pump frequencies are comparable to the zero-dispersion frequency (ZDF) of the fiber, a cascade of product waves (harmonics) is produced. In the low-pump-power regime that is characteristic of photon-generation experiments [10], weak harmonics are produced, which do not affect the primary process significantly. However, in the high-pump-power regime that is characteristic of signal-amplification experiments, strong harmonics are produced, which limit the level, and modify the phase sensitivity, of the signal gain. In this paper vector FWM is studied in detail. If the pumps are orthogonal,

#78120 - $15.00 USD Received 14 December 2006; revised 15 February 2007; accepted 15 February 2007

and the input-signal power is split evenly between the pump polarizations, vector FWM does not produce pump-pump harmonics, but does produce PSA with the aforementioned properties.

This paper is organized as follows: In Section 2 the coupled-mode equations (CMEs), which model wave propagation in a dispersionless RBF, are stated and solved for arbitrary input conditions. In Sections 3 and 4 these solutions are used to study pump–pump and pump–signal FWM cascades, respectively. Simulations that quantify the effects of dispersion are described in Section 5. Finally, in Section 6 the main results of this paper are summarized.

2. Wave propagation in a fiber

Wave propagation in a RBF is modeled by the coupled Schroedinger equations (CSEs)

$$-i\partial_z X = \beta(i\partial_\tau)X + \gamma(|X|^2+|Y|^2)X, \quad (1)$$
$$-i\partial_z Y = \beta(i\partial_\tau)Y + \gamma(|X|^2+|Y|^2)Y, \quad (2)$$

where z is distance, $\partial_z = \partial/\partial z$, X and Y are the amplitude (polarization) components of the wave and β is the dispersion function of the fiber. In the frequency domain $\beta(\omega) = \sum_{n\geq 2}\beta_n(\omega_c)\omega^n/n!$, where ω_c is the carrier frequency of the wave and ω is the difference between the actual and carrier frequencies. To convert from the frequency domain to the time domain one replaces ω by $i\partial_\tau$, where $\tau = t-\beta_1 z$ is the retarded time and $\beta_1(\omega_c)$ is the group slowness. The nonlinearity coefficient $\gamma = 8\gamma_K/9$, where γ_K is the Kerr coefficient. Equations (1) and (2) are valid in a frame that rotates randomly with the polarization axes of a reference wave. They omit the effects of polarization-mode dispersion [11], which are weak for the narrow spectral bandwidths and short fiber lengths of current experiments.

As stated in the Introduction, and discussed quantitatively in [9], if the frequencies of the interacting waves are comparable to the ZDF of fiber, the effects of dispersion are much weaker than those of nonlinearity and can be neglected. In this limit ($\beta = 0$), the CSEs reduce to the coupled-mode equations (CMEs)

$$\partial_z X = i\gamma(|X|^2+|Y|^2)X, \quad (3)$$
$$\partial_z Y = i\gamma(|X|^2+|Y|^2)Y, \quad (4)$$

which model the effects of self-phase modulation (SPM) and cross-phase modulation (CPM). The notation and language of this paper are based on the assumption that the basis vectors for the wave amplitude are linearly polarized. However, Eqs. (3) and (4) are valid for any pair of orthogonal vectors, including counter-rotating circularly-polarized vectors. Each polarization component depends implicitly on the retarded time.

The CMEs have the simple solutions

$$X(\tau,z) = X(\tau,0)\exp\big(i\gamma[|X(\tau,0)|^2+|Y(\tau,0)|^2]z\big), \quad (5)$$
$$Y(\tau,z) = Y(\tau,0)\exp\big(i\gamma[|X(\tau,0)|^2+|Y(\tau,0)|^2]z\big). \quad (6)$$

Because solutions (5) and (6) contain only the effects of nonlinearity, it is convenient to let P be a reference power, $X/P^{1/2}\to X$, $Y/P^{1/2}\to Y$ and $\gamma Pz\to z$, in which case the amplitude and distance variables are dimensionless, and γ is absent from the solutions.

3. Pump-pump cascade

Consider the two-frequency boundary (initial) conditions

$$X(\tau,0) = \rho_-\cos\theta_-\exp(i\phi_-)+\rho_+\cos\theta_+\exp(i\phi_+), \quad (7)$$
$$Y(\tau,0) = \rho_-\sin\theta_-\exp(i\phi_-)+\rho_+\sin\theta_+\exp(i\phi_+), \quad (8)$$

#78120 - $15.00 USD Received 14 December 2006; revised 15 February 2007; accepted 15 February 2007

where $\phi_+ = -\omega\tau + \phi_1(0)$ and $\phi_- = \omega\tau + \phi_{-1}(0)$. These conditions correspond to two pumps (± 1) with frequencies $\pm\omega$, which are inclined at the angles $\theta_\pm$ relative to the x-axis. (The average of the pump frequencies equals the carrier frequency.) The input power has the time average $\rho_+^2 + \rho_-^2$ and the contribution $2\rho_+\rho_- \cos(\theta_+ - \theta_-)\cos(\phi_+ - \phi_-)$, which oscillates at the difference frequency 2ω. The input power depends on the phase difference $\phi_d = [\phi_1(0) - \phi_{-1}(0)]/2$, but does not depend on the phase average $\phi_a = [\phi_1(0) + \phi_{-1}(0)]/2$. By measuring phase relative to the reference phase ϕ_a, and time relative to the reference time ϕ_d/ω, one can rewrite conditions (7) and (8) in the simpler forms

$$X(\tau,0) = \rho_- \cos\theta_- \exp(i\phi) + \rho_+ \cos\theta_+ \exp(-i\phi), \quad (9)$$

$$Y(\tau,0) = \rho_- \sin\theta_- \exp(i\phi) + \rho_+ \sin\theta_+ \exp(-i\phi), \quad (10)$$

where $\phi = \omega\tau$.

By using the identity $\exp(i\zeta\cos\psi) = \sum_m i^m J_m(\zeta)\exp(-im\psi)$ [12], where m is an integer, J_m is the Bessel function of order m, ζ is the distance parameter $2\rho_+\rho_-\cos(\theta_+ - \theta_-)z$ and ψ is the phase parameter 2ϕ, one can write solutions (5) and (6) as the series $X(\tau,z) = \sum_n X_n(z)\exp(-in\phi)$ and $Y(\tau,z) = \sum_n Y_n(z)\exp(-in\phi)$, respectively. The frequency components (harmonics)

$$X_n(\zeta) = \rho_- \cos\theta_- i^{(n+1)/2} J_{(n+1)/2}(\zeta) + \rho_+ \cos\theta_+ i^{(n-1)/2} J_{(n-1)/2}(\zeta), \quad (11)$$

$$Y_n(\zeta) = \rho_- \sin\theta_- i^{(n+1)/2} J_{(n+1)/2}(\zeta) + \rho_+ \sin\theta_+ i^{(n-1)/2} J_{(n-1)/2}(\zeta), \quad (12)$$

where n is an odd integer and the (common) phase factor $\exp[i(\rho_+^2 + \rho_-^2)z]$ was omitted for simplicity. For continuous-wave inputs $\rho_\pm$ are constant (as are ϕ_a and ϕ_d), whereas for pulsed inputs they vary slowly with time (as do ϕ_a and ϕ_d). As distance increases, so also does the number of harmonics (modes) with significant power: Eqs. (11) and (12) describe a vector FWM cascade. Notice that the mode powers $|X_n|^2$ and $|Y_n|^2$ do not depend on the input phases: This pump–pump cascade is phase insensitive (PI). Two other properties follow from Eqs. (11) and (12), and the identity $\sum_m J_m^2(\zeta) = 1$ [12]. First,

$$\sum_n |X(\zeta)|^2 = \rho_-^2 \cos^2\theta_- + \rho_+^2 \cos^2\theta_+, \quad (13)$$

which shows that the time-averaged power in the x-component is constant, consistent with solution (5). Second,

$$\sum_n [|X_n(\zeta)|^2 - |X_{-n}(\zeta)|^2] = (\rho_+^2 \cos^2\theta_+ - \rho_-^2 \cos^2\theta_-) J_0^2(\zeta), \quad (14)$$

which shows that the asymmetry in the x-component of the power spectrum decreases non-monotonically with distance (as $1/\zeta$). Similar results apply to the y-component.

The evolution of the pump–pump cascade is illustrated in Fig. 2, for the initial conditions $\rho_\pm = 1$ and $\theta_- = 0$. In each row the polarization components of the pump spectrum (pump spectra) are displayed for two distances, $z = 0$ and $z = 2$. The first row corresponds to pumps that are parallel initially ($\theta_+ = 0$), the second row corresponds to oblique pumps ($\theta_+ = \pi/4$) and the third row corresponds to perpendicular pumps ($\theta_+ = \pi/2$). Figures 2(a) and 2(b) show that, if the pumps are x-polarized initially, they remain x-polarized: The CMEs do not allow a transfer of power from one component to the other. If the pumps are oblique a FWM cascade also occurs. However, the cascade in Fig. 2(d) is less developed than the cascade in Fig. 2(b), because the oscillations in total power are weaker (ζ is smaller). If the pumps are perpendicular the total power is constant, so no cascade occurs, as shown in Fig. 2(f). It was shown in [13, 14] that perpendicular pumps in RBFs do not produce the lowest harmonics (modes -3 and 3). The

#78120 - $15.00 USD Received 14 December 2006; revised 15 February 2007; accepted 15 February 2007

preceding analysis shows that they produce no harmonics whatsoever. We validated the spectra displayed in Fig. 2 (and Figs. 3, 6 and 7) by calculating the Fourier transforms of solutions (5) and (6) numerically.

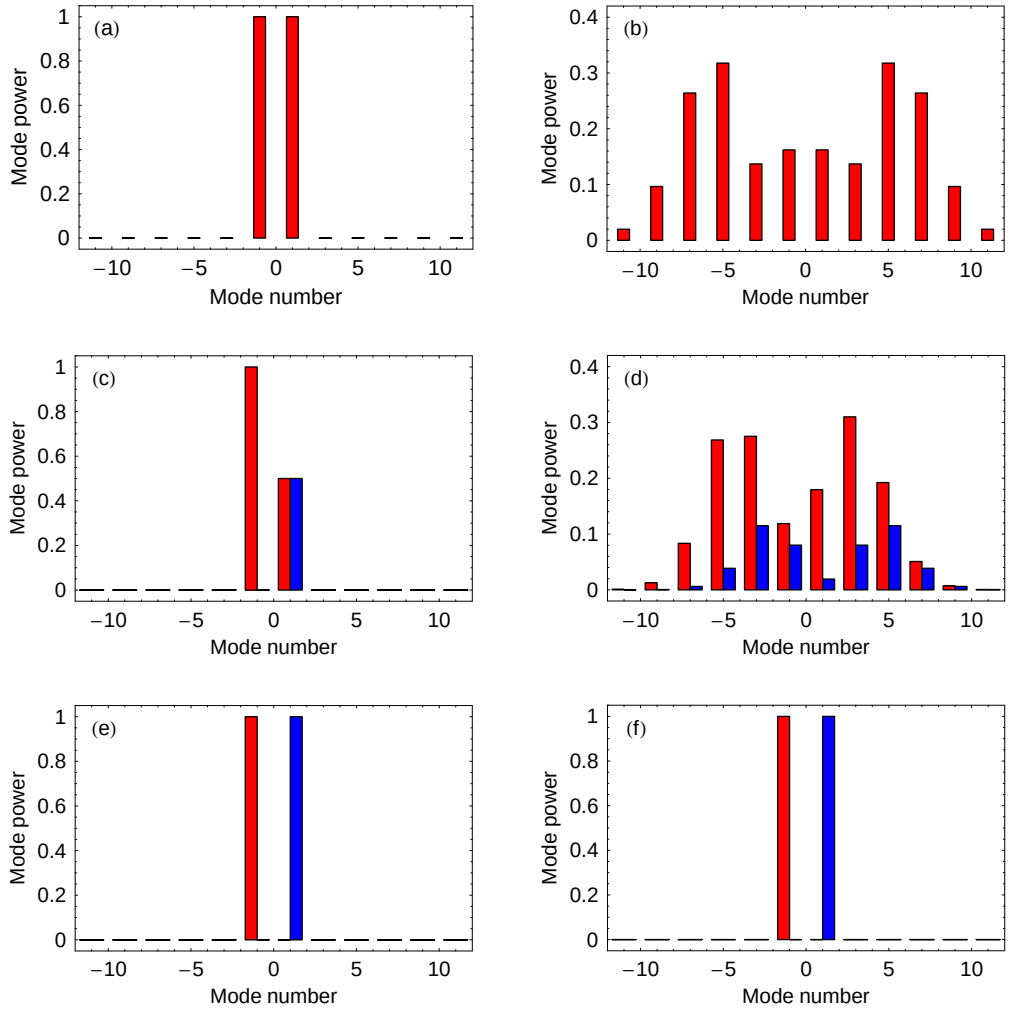

Fig. 2. Mode powers plotted as functions of mode number for cases in which the input amplitudes $\rho_{\pm} = 1$ and the input polarization-angle $\theta_{-} = 0$. The other angle $\theta_{+} = 0$ (top row), $\theta_{+} = \pi/4$ (middle row) and $\theta_{+} = \pi/2$ (bottom row), and the distance $z = 0$ (left column) and $z = 2$ (right column). Red (light-gray) bars represent x-components, whereas blue (dark-gray) bars represent y-components.

4. Pump-signal cascades

Now consider the three-frequency initial conditions

$$X(\tau,0) = \rho\exp(i\phi) + \rho_0\cos\theta_0\exp(i\phi_0), \quad (15)$$

$$Y(\tau,0) = \rho_0\sin\theta_0\exp(i\phi_0) + \rho\exp(-i\phi), \quad (16)$$

where ρ, ρ_0, θ_0 and ϕ_0 are constants (or slowly-varying functions of time). These conditions correspond to two pumps of equal power and a signal whose frequency is the average of the

#78120 - $15.00 USD Received 14 December 2006; revised 15 February 2007; accepted 15 February 2007

pump frequencies (0). The pumps are perpendicular and the signal is polarized at the angle θ_0 to pump -1. For these conditions, the input power has the time average $2\rho^2+\rho_0^2$ and the contribution $2\rho\rho_e\cos(\phi-\phi_e)$, which oscillates at the difference frequency ω. The (effective) amplitude and phase parameters

$$\rho_e = \rho_0[1+\sin(2\theta_0)\cos(2\phi_0)]^{1/2}, \quad (17)$$

$$\phi_e = \tan^{-1}[\tan\phi_0(1-\tan\theta_0)/(1+\tan\theta_0)]. \quad (18)$$

Notice that ρ_e, which determines the strength of the power oscillations, depends on ϕ_0, unless $\theta_0=0$ or $\pi/2$. By using the aforementioned identity, one can write solutions (5) and (6) as the series $X(\tau,z)=\sum_n X_n(z)\exp[-in(\phi-\phi_e)]$ and $Y(\tau,z)=\sum_n Y_n(z)\exp[-in(\phi-\phi_e)]$, respectively. The harmonics

$$X_n(\zeta) = i^{n+1}J_{n+1}(\zeta)\rho\exp(i\phi_e)+i^nJ_n(\zeta)\rho_0\cos\theta_0\exp(i\phi_0), \quad (19)$$

$$Y_n(\zeta) = i^{n-1}J_{n-1}(\zeta)\rho\exp(-i\phi_e)+i^nJ_n(\zeta)\rho_0\sin\theta_0\exp(i\phi_0), \quad (20)$$

where n is an integer, $\zeta=2\rho\rho_e z$ and the (common) phase factor $\exp[i(2\rho^2+\rho_0^2)]$ was omitted. Equations (19) and (20) describe a pump–signal cascade, and are valid for arbitrary signal polarizations and signal phases. In this paper the polarization dependence of the cascade is studied for the case in which $\phi_0=0$, and the phase dependence of the cascade is studied for the case in which $\theta_0=\pi/4$.

First, suppose that $\phi_0=0$. Then $\rho_e=\rho_0[1+\sin(2\theta_0)]^{1/2}$ and $\phi_e=0$ or π. These parameter specifications are equivalent to $\rho_e=\rho_0(\cos\theta_0+\sin\theta_0)$ and $\phi_e=0$. Equations (19) and (20) reduce to the simpler equations

$$X_n(\zeta) = i^{n+1}J_{n+1}(\zeta)\rho+i^nJ_n(\zeta)\rho_0\cos\theta_0, \quad (21)$$

$$Y_n(\zeta) = i^{n-1}J_{n-1}(\zeta)\rho+i^nJ_n(\zeta)\rho_0\sin\theta_0, \quad (22)$$

where ζ was defined after Eq. (20). Notice that the harmonics have x and y components for arbitrary θ_0: This pump–signal cascade is polarization diverse.

The evolution of the pump–signal cascade is illustrated in Fig. 3, for the initial conditions $\rho=1$, $\rho_0=0.1$ and $\phi_0=0$. In each row power spectra are displayed for two distances, $z=0$ and 4. The first row corresponds to a signal that is parallel to pump -1 initially ($\theta_0=0$), the second row corresponds to a signal that is polarized at 45° to the pumps ($\theta_0=\pi/4$) and the third row corresponds to a signal that is parallel to pump 1 ($\theta_0=\pi/2$). Power is normalized to 10^{-4}, so the input pump powers $P_{\pm1}=1$ correspond to 40 dB and the input signal power $P_0=0.01$ corresponds to 20 dB. Figures 3(a) and 3(b) show that an x-polarized signal produces an x-polarized pump–signal cascade. This cascade is similar to the cascade illustrated in Figs. 2(a) and 2(b), but is less developed, because the signal in the latter cascade is weaker than pump 1 in the former. Notice that a y-polarized cascade develops sympathetically, even though the y-component of the input power was not modulated. For $z=4$, only a slight asymmetry between the x- and y-components of this vector cascade exists (which is clearly visible in modes ±2). Similar remarks apply to Figs. 3(e) and 3(f), which illustrate the vector cascade produced by a y-polarized signal. The strongest vector cascade occurs when $\theta_0=\pi/4$, in which case the input signal power is split evenly between the pump polarizations, and the cascade that develops is symmetric. This case corresponds to the strongest modulation of the input power ($\rho_e=2^{1/2}\rho_0$).

Second, suppose that $\theta_0=\pi/4$. Then $\rho_e=2\hat{\rho}_0|\cos\phi_0|$, where $\hat{\rho}_0=\rho_0/2^{1/2}$, and $\phi_e=0$ or π. These parameter specifications are equivalent to $\rho_e=2\hat{\rho}_0\cos\phi_0$ and $\phi_e=0$. Equations (19) and (20) reduce to the simpler equations

$$X_n(\zeta) = i^{n+1}J_{n+1}(\zeta)\rho+i^nJ_n(\zeta)\hat{\rho}_0\exp(i\phi_0), \quad (23)$$

$$Y_n(\zeta) = i^{n-1}J_{n-1}(\zeta)\rho+i^nJ_n(\zeta)\hat{\rho}_0\exp(i\phi_0), \quad (24)$$

#78120 - $15.00 USD Received 14 December 2006; revised 15 February 2007; accepted 15 February 2007

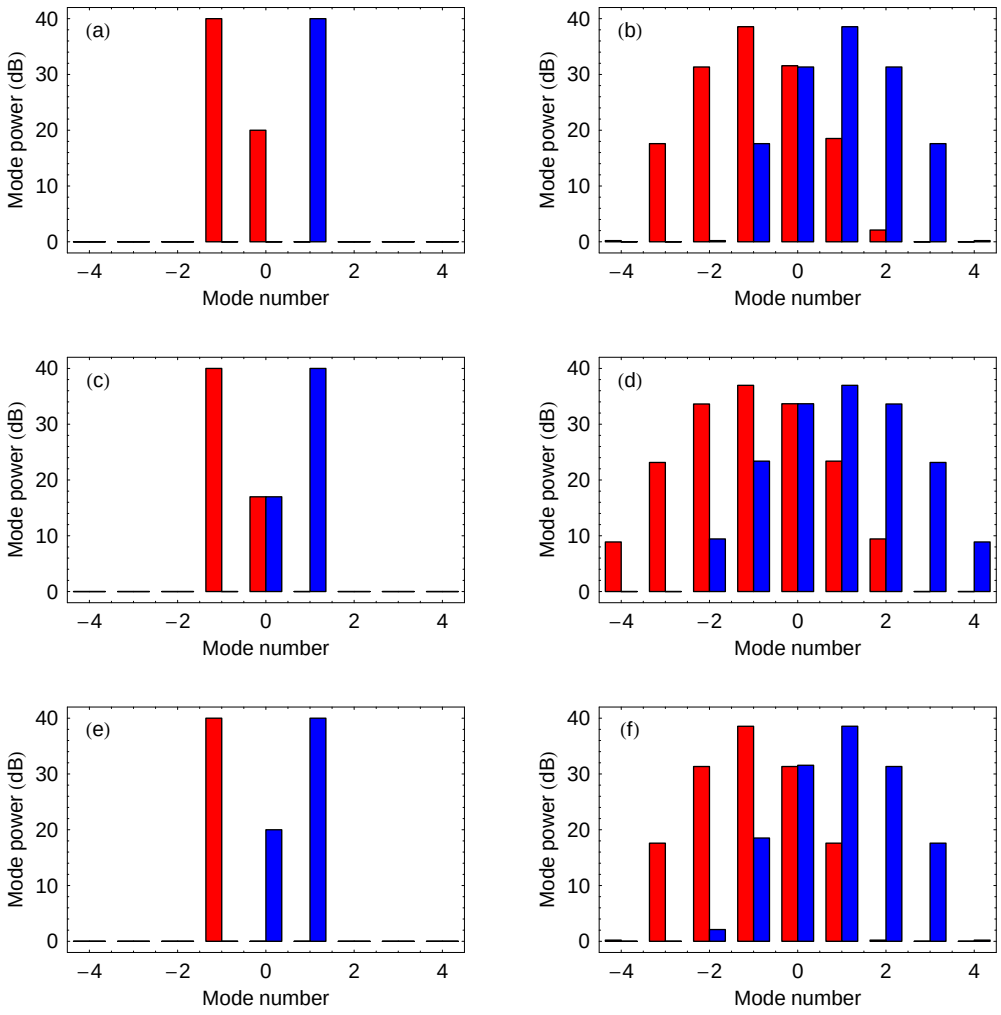

Fig. 3. Normalized mode powers plotted as functions of mode number for cases in which the input amplitudes $\rho = 1$ and $\rho_0 = 0.1$, and the input phase $\phi_0 = 0$. The input polarization-angle $\theta_0 = 0$ (top row), $\theta_0 = \pi/4$ (middle row) and $\theta_0 = \pi/2$ (bottom row), and the distance $z = 0$ (left column) and $z = 4$ (right column). Red bars represent x-components, whereas blue bars represent y-components.

where ζ was defined after Eq. (20). Notice that the harmonics depend on ϕ_0: This pump-signal cascade is phase sensitive (PS). It follows from Eq. (23) that

$$X_0(\zeta) = iJ_1(\zeta)\rho + J_0(\zeta)\hat{\rho}_0 \exp(i\phi_0). \tag{25}$$

The formula for Y_0 is identical. In the linear regime ($\zeta \ll 1$), the output signal is proportional to the input signal. (Because $\rho_0/\rho \ll 1$, it is possible that $\zeta \ll 1$ and $\rho^2 z \sim 1$ simultaneously.) In this regime,

$$X_0(z) \approx (1 + i\rho^2 z)\hat{\rho}_0 \exp(i\phi_0) + i\rho^2 z\hat{\rho}_0 \exp(-i\phi_0). \tag{26}$$

Although Eq. (26) is only part of an approximate solution of the CMEs, it is the exact solution of the FWM equations for the standard PS process [5, 6, 7], which involves only modes -1, 0

#78120 - $15.00 USD Received 14 December 2006; revised 15 February 2007; accepted 15 February 2007

and 1 [Fig. 1(*b*)]. It follows from Eq. (26), and its counterpart for Y_0, that the signal power

$$P_0(z) \approx \rho_0^2[1+2(\rho^2 z)^2+2(\rho^2 z)\sin(2\phi_0)+2(\rho^2 z)^2\cos(2\phi_0)]. \tag{27}$$

It follows from Eq. (27) that the signal gain $P_0(z)/\rho_0^2$ attains its extremal values when $2\phi_0 = \tan^{-1}(1/\rho^2 z)$. Let $\mu = 1+i\rho^2 z$ and $\nu = i\rho^2 z$. Then the first-quadrant value of $2\phi_0$ corresponds to the maximal gain $(|\mu|+|\nu|)^2$, whereas the third-quadrant value corresponds to the minimal gain $(|\mu|-|\nu|)^2$. It also follows from Eq. (23) that, in the linear regime,

$$X_{-2}(z) \approx i2\rho^2 z\hat{\rho}_0\cos\phi_0. \tag{28}$$

For long distances ($\rho^2 z > 1$), $X_{-2} \approx X_0$, unless $\phi_0 \approx \pi/2$ or $3\pi/2$. Similar results apply to Y_2.

The dependence of the signal power (gain) on phase and distance is illustrated in Fig. 4, for the initial conditions $\rho = 1$ and $\rho_0 = 0.01$ (which correspond to pump powers of 1 W and a signal power of 0.1 mW). The contour spacing is 2.5 dB, so the white regions correspond to positive gains higher than 18.75 dB, whereas the black region corresponds to negative gain lower than -18.75 dB. For short distances the gain is maximal when the input phase $\phi_0 \approx \pi/4$, whereas it is minimal when $\phi_0 \approx 3\pi/4$. In contrast, for long distances the maximal- and minimal-gain conditions are $\phi_0 \approx 0$ and $\phi_0 \approx \pi/2$, respectively. This behavior distinguishes FWM in a fiber from difference-frequency generation in a crystal, for which the maximal- and minimal-gain conditions are $\phi_0 = 0$ and $\phi_0 = \pi/2$, respectively, for all distances [8].

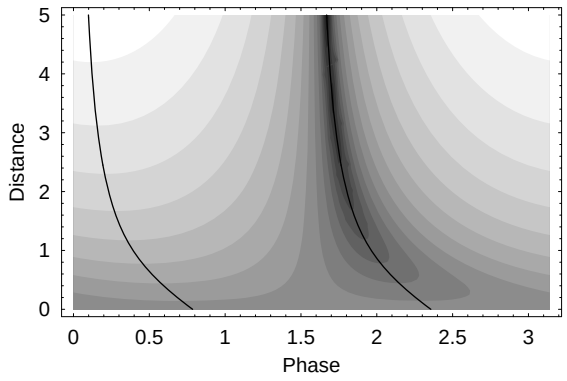

Fig. 4. Signal gain plotted as a function of input phase and distance. Light and dark regions correspond to positive and negative gains, respectively. The solid curves show the loci of maximal and minimal gain.

The dependence of the signal gain on phase and distance is also illustrated in Fig. 5, for the initial conditions $\rho = 1$ and $\rho_0 = 0.01$. In Fig. 5(*a*) the gain is plotted as a function of input phase, for the case in which $z = 5$. When $\phi_0 = 0$, the gain is $1+4(\rho^2 z)^2$: The signal power increases quadratically with distance. In contrast, when $\phi_0 = \pi/2$ the gain is 1: The signal is not amplified and no idlers are produced. The maximal gain $\{[1+(\rho^2 z)^2]^{1/2}+\rho^2 z\}^2 \approx 4(\rho^2 z)^2$ corresponds to $\phi_0 = 0.099$, whereas the minimal gain $\{[1+(\rho^2 z)^2]^{1/2}-\rho^2 z\}^2 \approx 1/4(\rho^2 z)^2$ corresponds to $\phi_0 = 1.67$. In Fig. 5(*b*) the gain is plotted as a function of distance, for the extremal cases in which $\phi_0 = 0.099$ and 1.67. The power of the amplified signal (normalized to 10^{-4}) increases from 1 to 102 (20.1 dB), whereas the power of the attenuated signal decreases from 1 to 9.8×10^{-3} (-20.1 dB). These results show that vector FWM provides (at least) 20 dB of PS amplification or attenuation. Neither process is impeded by the generation of idlers.

The evolution of the pump–signal cascade is illustrated in Fig. 6, for the initial conditions $\rho = 1$, $\rho_0 = 0.01$ and $\phi_0 = 0.099$ (maximal gain). Spectra are displayed for $z = 0$ and $z = 5$.

#78120 - $15.00 USD Received 14 December 2006; revised 15 February 2007; accepted 15 February 2007

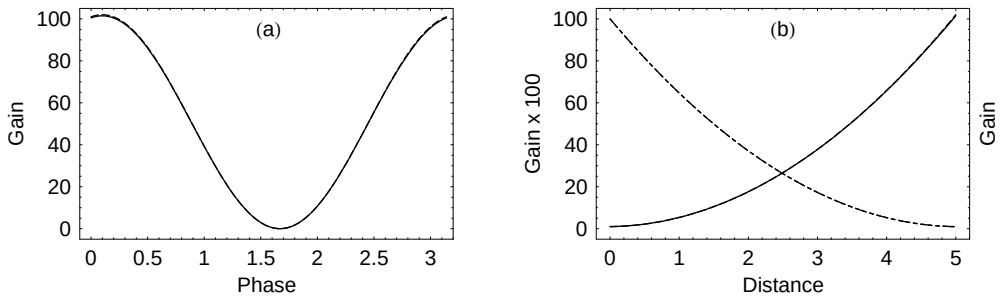

Fig. 5. Signal gain plotted as a function of input phase and distance for cases in which $\rho = 1$ and $\rho_0 = 0.01$: $z = 5$ (left), and $\phi_0 = 0.099$ and $\phi_0 = 1.67$ (right). In the phase plot the exact and approximate results are denoted by solid and dashed curves, respectively. In the distance plot they are represented by solid and dashed curves (amplification), and dot-dashed and dotted curves (attenuation). The exact and approximate curves are nearly indistinguishable.

Power is normalized to 10^{-6}, so the input pump powers $P_{\pm 1} = 1$ correspond to 60 dB and the input signal power $P_0 = 10^{-4}$ corresponds to 20 dB. (Each component of the signal has a power of 17 dB.) The output signal power is about 40 dB (37 dB in each component). In addition to a strong output signal, FWM produces two strong idler modes. Mode -2, which is *x*-polarized, is generated by the FWM processes in which $2\gamma_{-1} \rightarrow \gamma_{-2} + \gamma_0$ and $\gamma_{-1} + \gamma_0 \rightarrow \gamma_{-2} + \gamma_1$, and enhanced by the process in which $\gamma_{-1} + \gamma_1 \rightarrow \gamma_{-2} + \gamma_2$. Similar processes produce mode 2, which is *y*-polarized. The scalar pump–signal cascade produces many idlers, whose powers are comparable to the signal power, and whose presence limits the signal gain [9]. In contrast, the vector pump–signal cascade produces only two idlers, whose presence does not affect the signal gain significantly.

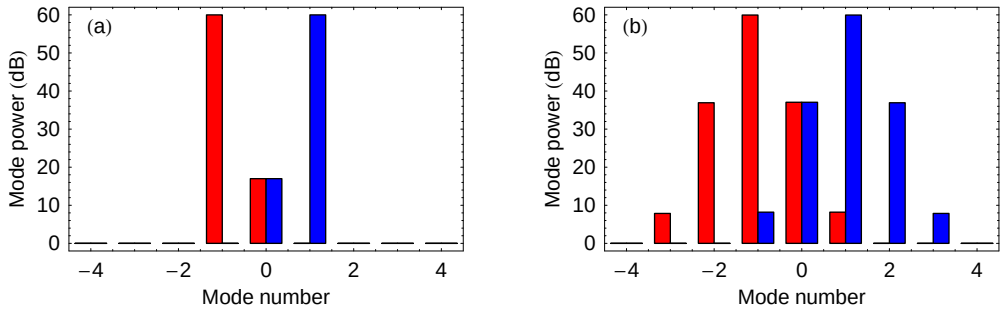

Fig. 6. Normalized mode powers plotted as functions of mode number for the case in which $\rho = 1$, $\rho_0 = 0.01$ and $\phi_0 = 0.099$: $z = 0$ (left) and $z = 5$ (right). Red bars represent *x*-components, whereas blue bars represent *y*-components.

Two other spectra are displayed in Fig. 7, for the initial conditions $\rho = 1$ and $\rho_0 = 0.01$, which were illustrated in Fig. 6(*a*), and the distance $z = 5$. Figure 7(*a*) corresponds to $\phi_0 = 1.57$, for which no cascade occurs: The mode powers are constants. Similar behavior is exhibited by the standard PS process [5, 6, 7] and the scalar cascade [9]. Figure 7(*b*) corresponds to $\phi_0 = 1.67$ (minimal gain). The signal is attenuated, consistent with Fig. 5(*b*). In the standard PS process the signal power is transferred to the pumps (± 1). However, in the vector cascade the signal power is transferred to the neighboring idlers (± 2). This behavior is consistent with Eqs. (26) and (28): For long distances, the condition $2\phi_0 = \tan^{-1}(1/\rho^2 z)$ is equivalent to the conditions

#78120 - $15.00 USD Received 14 December 2006; revised 15 February 2007; accepted 15 February 2007

$\sin\phi_0 \approx 1$ and $\cos\phi_0 \approx -1/2\rho^2 z$, which imply that $X_0 \approx -\hat{\rho}_0/2\rho^2 z$ and $X_{-2} \approx -i\hat{\rho}_0$.

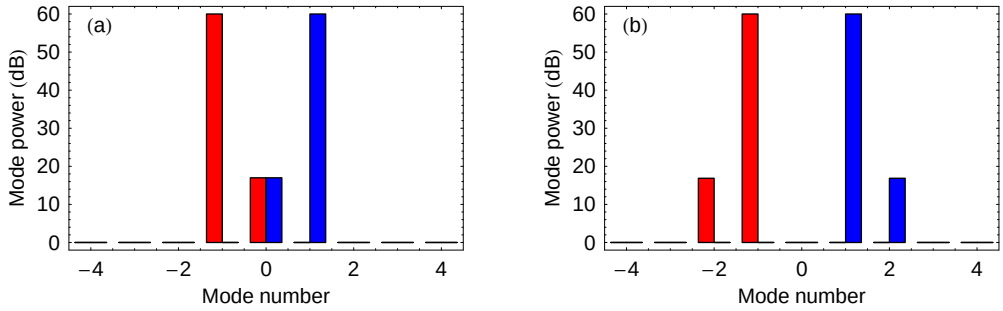

Fig. 7. Normalized mode powers plotted as functions of mode number for cases in which $\rho = 1$, $\rho_0 = 0.01$ and $z = 5$: $\phi_0 = 1.57$ (left) and $\phi_0 = 1.67$ (right). Red bars represent x-components, whereas blue bars represent y-components.

5. Numerical simulations of vector four-wave mixing

Current experiments involve highly-nonlinear fibers with dispersion coefficients $\beta_3 \approx 0.03$ ps^3/Km and $\beta_4 \approx -3 \times 10^{-4}$ ps^4/Km, nonlinearity coefficients $\gamma \approx 10$/Km-W (all evaluated at the ZDFs), and pumps with powers $P \approx 0.3$ W. The mode frequencies depend on the intended application. We chose (real) frequency spacings of 50 and 200 GHz (0.4 and 1.6 nm), which are the channel spacings for 10- and 40-Gb/s systems, respectively.

To check the analysis of Sections 3 and 4, we solved the CSEs numerically, using the standard split-step method, for the initial conditions of Figs. 2, 3, 6 and 7. In the absence of dispersion ($\beta_3 = 0$ and $\beta_4 = 0$), the numerical results agree with the analytical predictions (to the limit of numerical accuracy). In the presence of dispersion (with the aforementioned characteristics), there are some quantitative differences, but no qualitative differences, between the numerical results and the analytical predictions.

The evolution of the pump–pump cascade is illustrated in Fig. 8, for the initial conditions $\rho_\pm = 1$ and $\theta_- = 0$, and the distance $z = 2$. The total mode power is plotted as a function of mode number. Figure 8(a) corresponds to $\theta_+ = 0$, which was illustrated in Fig. 2(a). For a frequency spacing of 50 GHz, the difference between the numerical results and the analytical predictions does not exceed 0.8%. For a spacing of 200 GHz, moderate differences are visible. Dispersion breaks the symmetry between the positive- and negative-mode powers. However, it

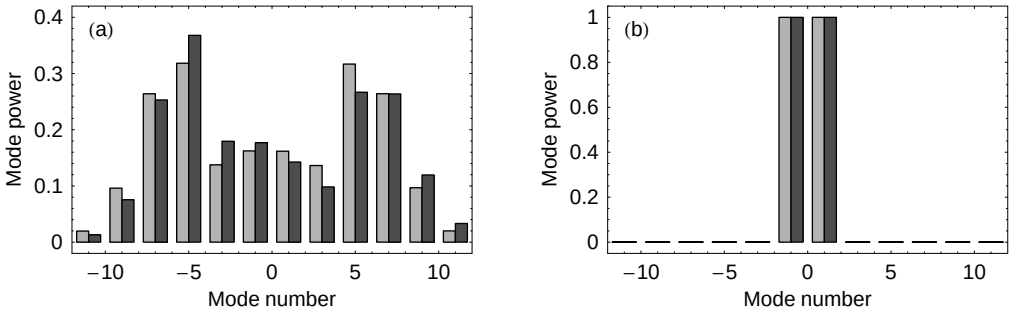

Fig. 8. Normalized mode powers plotted as functions of mode number for cases in which $\rho_\pm = 1$, $\theta_- = 0$ and $z = 2$: $\theta_+ = 0$ (left) and $\theta_+ = \pi/2$ (right). Light- and dark-gray bars correspond to frequency spacings of 50 and 200 GHz, respectively.

#78120 - $15.00 USD Received 14 December 2006; revised 15 February 2007; accepted 15 February 2007

is not strong enough to suppress the cascade driven by parallel pumps. Figure 8(*b*) corresponds to the initial condition $\theta_+ = \pi/2$, which was illustrated in Fig. 2(*e*). For both spacings, the numerical results agree with the analytical predictions: Perpendicular pumps do not produce a cascade.

The evolution of the pump–signal cascade is illustrated in Fig. 9, for the initial conditions $\rho = 1$ and $\rho_0 = 0.01$, which were illustrated in Fig. 6(*a*), and the distance $z = 5$. The total mode power is plotted as a function of mode number. Figure 9(*a*) corresponds to $\phi_0 = 0.099$ (maximal gain in the zero-dispersion limit). For a frequency spacing of 50 GHz, the difference between the numerical results and the analytical predictions does not exceed 0.5%. For a spacing of 200 GHz, small differences in the powers of modes -3 and 3 are visible. However, for both spacings the signal is amplified by 20 dB. Figure 9(*b*) corresponds to $\phi_0 = 1.67$ (minimal gain in the zero-dispersion limit). For both spacings, the numerical results agree with the analytical predictions: The signal is attenuated by 20 dB.

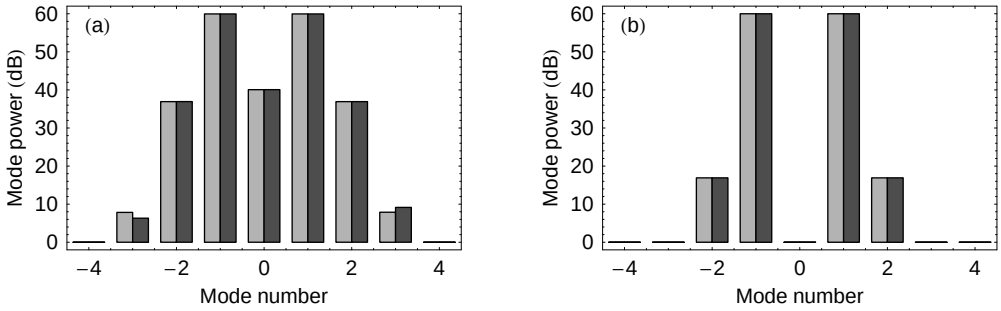

Fig. 9. Normalized mode powers plotted as functions of mode number for cases in which $\rho = 1$, $\rho_0 = 0.01$ and $z = 5$: $\phi_0 = 0.099$ (left) and $\phi_0 = 1.67$ (right). Light- and dark-gray bars correspond to frequency spacings of 50 and 200 GHz, respectively.

As the frequency spacing increases, so also do the differences between the numerical results and the analytical predictions. However, it remains true that perpendicular pumps do not produce a cascade, and a signal polarized at 45° to such pumps experiences significant PS amplification or attenuation. The extremal-gain conditions depend on the frequency spacing.

6. Summary

In this paper studies were made of the frequency cascades initiated by two strong pump waves (-1 and 1), and two strong pump waves and a weak signal wave (0), whose frequency is the average of the pump frequencies. These cascades are produced by vector four-wave mixing (FWM) in a randomly-birefringent fiber (RBF).

Wave propagation in a RBF is governed by coupled Schroedinger equations (CSEs). However, if the frequencies of the interacting waves are comparable to the zero-dispersion frequency (ZDF) of the fiber, the effects of dispersion are much weaker than those of nonlinearity and can be neglected. In this limit, the CSEs reduce to the coupled-mode equations (3) and (4), which were solved exactly.

The pump–pump cascade [Eqs. (11) and (12)] is phase insensitive. Parallel pumps produce a strong cascade with many harmonics. However, as the pump misalignment increases, the number and strength of the harmonics decrease. Perpendicular pumps do not produce a cascade.

The absence of a pump–pump cascade modifies the properties of the associated pump–signal cascade [Eqs. (17) and (18)], which is phase sensitive. If the signal is polarized at 45° to the pumps, only two strong harmonics (idlers) are produced (-2 and 2). These idlers are produced

#78120 - $15.00 USD Received 14 December 2006; revised 15 February 2007; accepted 15 February 2007

by the pumps and signal, but do not affect the signal adversely: For parameters that are typical of current experiments, the signal can be amplified or attenuated by more than 20 dB, depending on its input phase.

The analytical predictions of this paper were validated by numerical simulations based on the CSEs, which included the effects of dispersion.

In conclusion, vector FWM near the ZDF of a RBF produces phase-sensitive amplification with the classical properties of a one-mode squeezing transformation. This result is important, because it is easier to phase-lock pumps with similar frequencies (produced by one laser and a phase modulator) than pumps with dissimilar frequencies (produced by two separate lasers).

Acknowledgments

The research of SR and MR was supported by the National Science Foundation, under contracts ECS-0406379 and PHY-0456974, respectively.

#78120 - $15.00 USD Received 14 December 2006; revised 15 February 2007; accepted 15 February 2007